Experimental Study on Styrene-Butadiene-Styrene Modified Binders and Fly Ash Micro-Filler Contributions for Implementation in Porous Asphalt Mixes

Manuel Lagos-Varas , Diana Movilla-Quesada * , Aitor C. Raposeiras , Melany Villarroel , Ana B. Ramos-Gavilán , Daniel Castro-Fresno

Posted Date: 21 December 2023

doi: 10.20944/preprints202312.1644.v1

Keywords: Porous asphalt mixes; Styrene-butadiene-styrene; fly ashes; bitumen; rheology

Article

Experimental Study on Styrene-Butadiene-Styrene Modified Binders and Fly Ash Micro-Filler Contributions for Implementation in Porous Asphalt Mixes

Manuel Lagos-Varas [1,4], Diana Movilla-Quesada [2,*], Aitor C. Raposeiras [3], Melany Villarroel [4], Ana B. Ramos-Gavilán [3] and Daniel Castro-Fresno [1]

[1] GITECO Research Group, University of Cantabria, Av. Los Castros, 39005 Santander, Spain; dcastro@unican.es
[2] Departamento de Construcción y Agronomía, Escuela Politécnica Superior de Zamora, Universidad de Salamanca, 49029 Zamora, España; dmovilla@usal.es
[3] Departamento de Ingeniería Mecánica, Escuela Politécnica Superior de Zamora, Universidad de Salamanca, 49029 Zamora, España; araposeiras@usal.es, aramos@usal.es
[4] Gi²V Research Group, Institute of Civil Engineering, Faculty of Engineering Sciences, University Austral of Chile, Valdivia, Chile; manuel.lagos@uach.cl, melany.villarroel@alumnos.uach.cl
* Correspondence: dmovilla@usal.es

Abstract: Butadiene-Styrene copolymer (SBS) to improve the mechanical and deformation properties of the binder used in its manufacture. However, the high cost and variability of processing limit its performance. A secondary modifier to solve these problems is nano and micro materials that allow the generation of unique properties in polymeric systems. Based on this, this study experimented with fly ash micro filler ((μFA) in low proportions as a binder modifier with SBS for use in PA mixes. The FA residue is considered in 3% and 5% dosages on a base binder with 5% SBS. Rheological results show that μFA improves classical, linear viscoelastic (LVE), and progressive damage properties compared to the modified binder. The PA blends with μFA reduced binder runout, resulting in a thicker film, showing better abrasion resistance in dry and wet conditions. Samples with μFA increase the post-cracking energy in indirect tension due to higher ductility. However, they decrease the fracture energy due to higher cracking before failure. In addition, the μFA manages to decrease the difference between dry and wet ITS.

Keywords: porous asphalt mixes; styrene-butadiene-styrene; fly ashes; bitumen; rheology.

1. Introduction

Porous asphalt (PA) is a type of flexible pavement used worldwide. Its unique properties allow for better safety, excellent slip resistance, lower noise, and greater comfort than other mixes [1]. PA mixes have an open grain size structure, allowing water to pass through the air voids (AV), generally greater than 20% [2]. This reduces the risk of water accumulation on the surface of the wearing course, thus contributing to stormwater management and reduction of hydroplaning, among other advantages [3]. Despite achieving good permeability, PA mixes achieve lower mechanical resistance than other types of mixes due to the limited amount of fine aggregate, which generates significant problems in the pavement, such as segregation, short-long term ageing, and moisture damage [4]. Therefore, despite the benefits of a PA, there are still challenges in the research for its correct implementation. One of the most addressed lines is the development of new modified binders for PA mixes. It has been shown that modified binders can contribute to failure prevention, improving mechanical properties and deformations. The most used modifiers are polymers (elastomers and thermoplastics), waxes, and special additives [5]. Styrene-butadiene-styrene copolymer (SBS) is the modifier that has generated the greatest revolution in the asphalt industry [6]. Adding SBS to the conventional binder confers a higher softening point and lower penetration rate [7]. In addition,

under linear viscoelasticity properties (LVE), it allows an increase in the dynamic modulus |G*| and delays the increase of the lag angle δ, providing a higher stiffness and elasticity [8]. Concerning the properties originated in progressive damage methodology, SBS achieves a higher recovery capacity, reducing the thermal susceptibility and reaching a higher integrity. About asphalt mixes, SBS improves permanent deformations, moisture damage, and cohesion between aggregate and binder, among others [9]. However, due to its high cost and problems with processing, mixing, segregation, and compatibility with other additives, other alternatives have been sought to replace this material totally or partially [7].

The incorporation of different types of filler in PA mixes significantly influences mechanical properties and durability [10]. The filler is considered a mineral material that can pass through the 0.075mm sieve and varies in shape, texture, size, and physical and chemical properties [11]. The filler and the binder form the asphalt mastic, which allows the actual agglomeration of the larger aggregates [12]. This matrix is relevant due to the dispersion of the filler in the binder matrix and the interaction it achieves in the microstructure of the porous asphalt [13]. Some studies have pointed out that water damage in asphalt mixes directly relates to the filler/binder interface. One of the most used fillers is limestone, primarily composed of calcium oxide (CaO), giving rise to adequate behaviour in humid climates [11]. However, due to environmental protection and increased production costs, new alternatives to replace this filler with other recycled materials have been studied [14]. One of the alternatives with excellent projection is using residues such as fly ash (FA) as fillers [15]. FA is a residue from pulverised coal combustion in power plants, of which only 25% is used [16]. This type of filler increases mechanical strength and improves stability by 3-6% in asphalt mixes [17]. FA filler has a thicker absorbed film than other fillers, such as limestone (L), showing good physical-chemical interaction with binder [18]. It has been shown that FA filler in hot mix asphalt (HMA) up to 4% reduces the optimum binder content by 7.5% compared to calcareous fillers [19]. Using Rigden voids (RV), it has even been demonstrated that the FA filler is more mechanically efficient than mastics with traditional fillers [12]. However, some authors have demonstrated the incompatibility of some fillers with the matrix, which generates serious adhesion problems. Thus, the difference between the elastic properties of the filler and binder generates a differential stress, which would eventually lead to fatigue failure of the material. Moreover, it is known that the macro mechanical behaviour of asphalt mixes is conditioned by the morphology and physical properties of the micro levels of the mixture (filler/binder) [20].

A practice that has become relevant is the use of micro or nanomaterials that allow the generation of unique properties in polymeric systems to achieve a high surface/volume ratio [21]. One example is nano clays, which are used as a secondary modifier to improve the bituminous binder's properties further [22]. Studies have shown that nano clay, in combination with an SBS binder, can increase the viscosity and complex modulus |G*| and decrease the angle d [23]. In addition, it is shown that nano clay has a promising potential to reduce permanent deformations. Another modifier is nano-silica, which can improve the anti-ageing performance, fatigue, rutting, and anti-tearing properties of asphalt binder [24]. Mojtaba et al. demonstrated that when 2% nano-SiO2 is added with 5% SBS improves the mechanical performance of asphalt mixes [25]. Similarly, Roman and Garcia-Morales studied a type of siliceous microfilter (lower than 100μm) and nanoclay (lower than 8 μm) in asphalt mastics, where they showed that a combined addition of standard filler and nanoclay has a positive effect on permanent deformation [22]. Furthermore, they concluded that 40% siliceous micro filler and 5% nano clay had a higher |G*| than a combination of only 45% micro filler for PMB.

Despite the advantages of nano or micro materials in asphalt binders, deepening the knowledge of their behaviour in asphalt mixes is still necessary. This is because nanoclays have disadvantages in moisture sensitivity, which is relevant for PA mixes. Likewise, nanosilicas generate excessive stiffness, which could cause problems segregating a PA mixture. Therefore, the main objective of this paper is to determine the influence of fly ash (FA) micro filler in Styrene-Butadiene-Styrene (SBS) modified binders for its implementation in a porous PA16 mix. The methodology proposed for this work is based on tests for asphalt binders (Penetration, Dynamic Shear Rheometer (DSR), Multiple

Preprints (www.preprints.org) | NOT PEER-REVIEWED | Posted: 21 December 2023 doi:10.20944/preprints202312.1644.v1

Stress Creep Recovery (MSCR), Linear Amplitude Sweep (LAS), and Binder Yield Energy (BYET)) and in PA mix (Binder et al. Test, Water Sensitivity Test, and the Cantabro test).

2. Materials and Methods

2.1. Materials

2.1.1. Aggregates

The aggregates used in this study are used to manufacture asphalt mixes in northern Spain. Ophite, a porphyritic igneous rock, was used as coarse aggregate, and limestone as fine aggregate and filler (Figure 1). The physical properties of both aggregates are shown in Table 1.

Figure 1. Aggregate limestone and ophite.

Table 1. Properties of aggregates.

Properties	Result	Limits	Standard
Limestone			
Los Angeles coefficient	28	-	EN 1097-2
Specific weight (g/cm^3)	2.724	-	EN 1097-6
Sand equivalent	78	>55	EN 933-8
Ophite			
Los Angeles coefficient	13	≤20	EN 1097-2
Specific weight (g/cm^3)	2.794	-	EN 1097-26
Polished stone value (PSV)	>56	≥50	EN 1097-8
Flakiness Index (%)	8	≤20	EN 933-3
Water absorption	0.60	-	EN 1097-6

2.1.2. Asphalt binder and modifiers

The asphalt binder used is type B50/70. The mechanical and physical properties are shown in Table 2. The first modifier used is the SBS copolymer supplied by Dynasol (Table 3). The second material used in the wet modification was a micro filler from fly ash (see Table 3). To obtain this material, a particle size of the FA filler was first generated (Table 4 and Figure 2a). Next, the material sifted through the 0.015 mm sieve was used, which accounted for 6.55% of the total mass of the FA filler. Thus, this document names fly ash micro filler (μFA) particles of dimension less than 15μm (Figure 2b).

Table 2. Properties of B50/70 bitumen.

Test	Units	Result	Standard
Penetration (25ºC)	dmm	65	EN 1426
Softening point	ºC	48.8	EN 1427
Density	g/cm^3	1.045	EN 15326
Penetration Index	-	-1.0	EN 12591

Preprints (www.preprints.org) | NOT PEER-REVIEWED | Posted: 21 December 2023 doi:10.20944/preprints202312.1644.v1

Four types of samples were prepared for the rheology tests on asphalt binders. The first sample is the standard and contains only B50/70. The second sample is B50/70 plus the addition of 5% SBS. The third and fourth samples are based on a modification of 5% SBS plus the incorporation of μFA at 3% and 5% by weight of B50/70 binder.

Table 3. Physical properties of SBS copolymer and FA filler.

Test	Units	Result	Standard
Styrene-Butadiene-Styrene			
Size max.	mm	6.3	-
Specific weight	g/cm^3	0.93	-
Type	-	Block Copolymer	-
Provider	-	Dynasol	-
Fly ash filler			
Density	g/cm^3	2.450	-
Rigden voids	%	73	-

The manufacturing process of the modified binders is carried out at 170ºC after heating the base binder. Mixing is generated in a homogenizer for 60 minutes at 1800 rpm. The SBS copolymer was added at the beginning of the process, and the μFA were added in the last 30 minutes with their respective dosage percentages. Subsequently, 25 mm and 8 mm cylindrical samples were created and tested in a Dynamic Shear Rheometer (DSR) according to the methodologies.

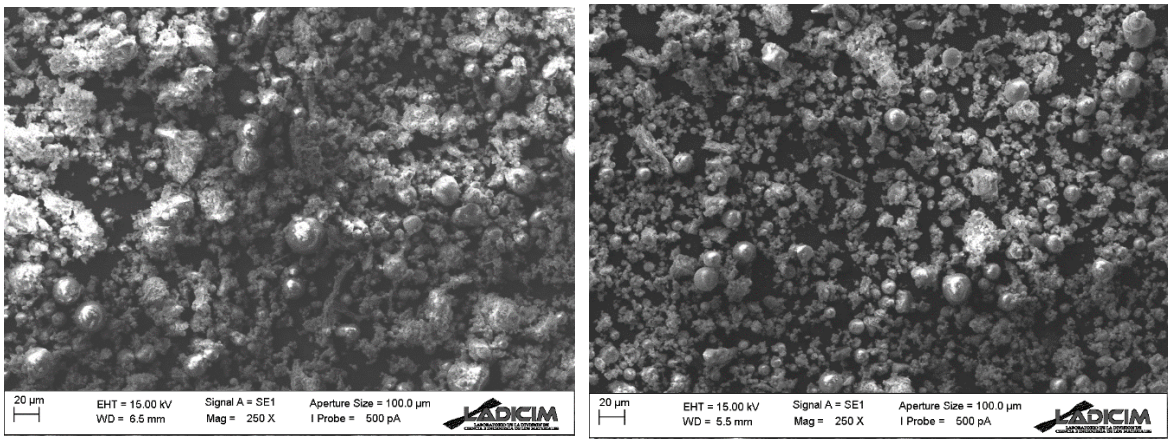

Figure 2. SEM images at 250x of Fly Ash. a) Filler FA; b) Micro filler FA.

2.1.3. Asphalt mixes

Porous asphalt mixes were designed using a PA16 particle size (see Figure 3). The PA samples were manufactured to reproduce the conventional process at 170ºC. The standard sample was B50/70+5%SBS because PA is typically used with polymer-modified binders for high traffic conditions (>800 heavy vehicles/day) according to the Spanish technical indications PG-3.

Preprints (www.preprints.org) | NOT PEER-REVIEWED | Posted: 21 December 2023 doi:10.20944/preprints202312.1644.v1

Table 4. FA filler particle size analysis.

Size (mm)	0.063	0.056	0.050	0.040	0.032	0.025	0.015
Passed Through (%)	84.68	69.34	57.03	39.57	19.80	9.55	6.55

The design and determination of the optimum binder content (OBC) was carried out for the standard sample using the Marshall design. The optimum percentage of binder in the aggregate was 4.7%.

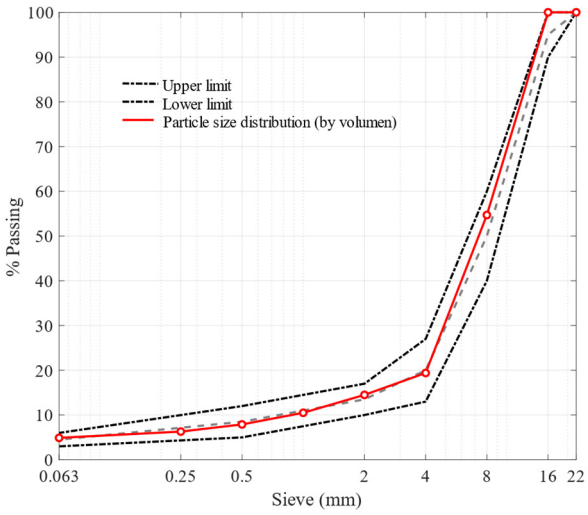

Figure 3. Design curve for PA16 mixes.

2.2. Methodology

2.2.1. Penetration

The penetration test is based on a test at 25±1°C. The test involves the determination of the consistency of the asphalt binder, expressed as the distance a steel needle vertically penetrates a sample of asphalt binder. The mass of the needle is 100g, and the test duration is 5±0.1 seconds. The penetration test is performed by UNE-EN1426.

2.2.2. Dynamic shear Rheometer (DSR) test

The DSR methodology determines the linear visco-elastic (LVE) properties of asphalt binders. The test is set up with a temperature sweep from 10°C to 70°C and a range from 0.1 to 30 Hz, with a sinusoidal displacement of 0.1% of strain. Parallel 25 mm plates are used for temperatures between 30 to 70°C, and parallel 8 mm plates are used for temperatures between 10 to 30°C. The height and spacing established between the plates is 1 mm. Modelling is performed by applying the master curve fitting to the obtained parameters, vector and complex modulus $|G^*|$ (Equation 1), and angle lag δ are obtained. Finally, for the temperature of 30°C, a superposition is performed for the two plates with a difference of less than 5%.

$$\log(|G^*|) = \alpha + \frac{\beta}{1 + e^{\rho - \gamma \log \omega_r}} \quad (1)$$

where α is the minor asymptote, β is the difference between the minor and major value of the asymptotes, ω_r is the reduced frequency, γ is the slope of the curve, and ρ is the inflection point.

Preprints (www.preprints.org) | NOT PEER-REVIEWED | Posted: 21 December 2023 doi:10.20944/preprints202312.1644.v1

2.2.3. Multiple stress creep and recovery (MSCR)

The MSCR test is performed on the base binder and the modified samples for temperatures of 30°C, 40°C, 50°C, 60°C and 70°C. DSR is used with 25 mm parallel plates with a 1 mm gap. The MSCR consists of 10 creep and recovery cycles of 1s and 9s, respectively. First, an applied load is applied at 0.1 kPa conditioning. Subsequently, the test is performed with a load of 3.2 kPa. The record of the accumulated deformations is used to obtain the elastic yield (R) and the unrecoverable creep (Jnr). These parameters are expressed in equations (2) and (3) [26]:

$$R_\sigma(\%) = \frac{1}{10}\sum_{i=1}^{10}\frac{\gamma_{p_i} - \gamma_{n_i}}{\gamma_{p_i} - \gamma_{0_i}} \tag{2}$$

$$J_{nr,\sigma}(1/kPa) = \frac{1}{10}\sum_{i=1}^{10}\frac{\gamma_{n_i} - \gamma_{0_i}}{\sigma} \tag{3}$$

where σ is the applied tensile stress, γ0 the strain at the beginning of the cycle, γp is the maximum strain after 1s of loading and γn is the non-recoverable strain at the end of the cycle after 9s of recovery.

2.2.4. Linear Amplitude Sweep (LAS)

The LAS test is performed for temperatures of 20°C and 25°C. The 8mm parallel plates of the DSR with a 2mm gap are used. The test consists of (1) applying a frequency sweep from 0.2Hz to 30Hz at a constant strain of 0.1%, then (2) increasing the strain from 0.1% to 30% at a constant frequency of 10Hz. Visco-Elastic Continuum Damage (VECD) modelling is applied to the tested samples to investigate the fatigue behaviour. This simulation is based on the relationship between the material integrity (C) and the Damage (D) caused. The damage evolution law [27]:

$$\frac{dD}{dt} = \left(-\frac{\partial W}{\partial D}\right)^{\alpha} \tag{4}$$

where W is the work done, t is the time, and α is the rate of damage evolution. By solving Eq. (4) and using the data obtained in the two test processes, the characteristic damage relationship is obtained, where the integrity (C=|G*|sin(δ)) is related to the damage intensity. The intensity and fatigue life are shown in equations (5) and (6), respectively:

$$D(t) \cong \sum_{i=1}^{N}[\pi{\gamma_0}^2(C_{i-1} - C_i)]^{\frac{\alpha}{1+\alpha}}(t_i - t_{i-1})^{\frac{1}{1+\alpha}}, \tag{5}$$

$$N_f = A \cdot (\gamma_{max})^{-B} \tag{6}$$

where *Nf* is the fatigue life, A and B are coefficients of the VECD model that depend on the material characteristics.

2.2.5. Binder Yield Energy (BYET) test

The BYET applies a load with a constant strain rate of 2,315 s-1 on the DSR. This research uses a test temperature of 20°C and 25°C. The stress and strain are recorded until 3600% strain is reached in 60 minutes. The parameters related to creep energy (Er) and strain at maximum shear stress are obtained. Er is calculated as the area under the stress-strain curve up to the point of maximum stress.

2.2.6. Binder Braindown

The test is performed by adding a non-compacted PA16 sample to a standardized mesh. For this purpose, about 1 kg of the mixture was added in an oven for 3 hours plus minus 15 minutes at the maximum mixing temperature (170ºC) plus 15ºC or 25ºC, depending on whether it is a modified or

Preprints (www.preprints.org) | NOT PEER-REVIEWED | Posted: 21 December 2023 doi:10.20944/preprints202312.1644.v1

conventional binder, respectively. The test is expressed as the percentage of drained binder concerning the initial and final mass, according to the following equation (UNE-EN12697-18).

$$B_d(\%) = \frac{b}{m} \quad (7)$$

where Bd is the percentage of binder draindown, b (g) is the amount of binder drained and m (g) is the mass of the mixture.

2.2.7. Volumetric test

The volumetric procedure determines the air voids in porous mixes according to the European standard UNE-EN12687-8. The purpose is to evaluate the internal structure of the mixes since they play an essential role in the mechanical performance of flexible pavements [28].

2.2.8. Water Sensitivity test

The water sensitivity test was performed by dividing the samples into two groups. The group of dry samples was stored at an ambient temperature of 20ºC. The wet sample group was subjected to a vacuum (6.7±0.3 kPa in 10 minutes). Subsequently, the wet samples were immersed in a water bath for 72 hours at 40ºC. Finally, the two groups were brought to a test temperature of 15ºC according to the Spanish standard (PG-3) and the indirect tensile strength ratio (ITSR) was calculated according to [29]:

$$ITS = \frac{2p}{\pi DH} \quad (8)$$

$$ITSR = \frac{ITS_w}{ITS_d} \quad (9)$$

where ITS is the indirect tensile strength (kPa), P is the maximum load (kN), D is the sample diameter (mm), H is the sample height (mm), ITS_w is the indirect tensile strength of wet samples and ITS_d is the tensile strength of dry samples, both in kPa.

2.2.9. Cantabrian particle loss test

The Cantabro particle loss test evaluates the loosening resistance of porous asphalt mixes [30]. For this purpose, the test measures the percentage mass loss of a Marshall sample subjected to abrasion in the Angels machine. The mass loss is expressed as the percentage after 300 revolutions, from the following equation:

$$\boldsymbol{Particle\ loss}\ (\%) = \frac{\boldsymbol{m_i - m_f}}{\boldsymbol{m_i}} \quad (10)$$

where m_i (g) is the initial mass and m_f (g) is the final mass. The test is performed for wet and dry samples. The wet samples were immersed in a water bath at 60ºC for 24 hours. Finally, the wet and dry samples were conditioned at 25ºC for 24 hours prior to testing.

3. Results and discussion

3.1. Penetration

The results of the penetration test are shown in Figure 4. It is demonstrated that incorporating 5% SBS into the B50/70 binder generates a reduction from 65 (0.1mm) to 36 (0.1mm). Thus, it is shown that SBS gives rise to a harder consistency in B50/70. By adding µFA at 3% and 5% the penetration further decreases to 33(0.1mm) and 31(0.1mm), respectively. This could be due to the elastic capacity delivered by the solid particles of µFA, which it will depend on their dispersion in the binder matrix.

Preprints (www.preprints.org) | NOT PEER-REVIEWED | Posted: 21 December 2023 doi:10.20944/preprints202312.1644.v1

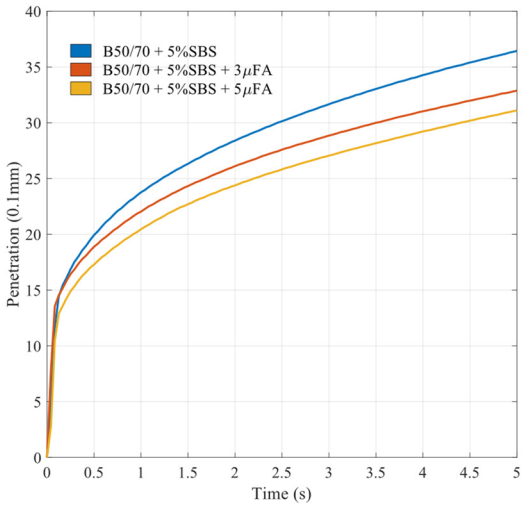

Figure 4. Results of penetration test.

3.2. DSR test

The results of the LVE properties determine that SBS increases the stiffness vector |*G**| of B50/70, where the most drastic changes are generated at high temperatures (see Table 5). However, when incorporating 3% of μFA to the sample with 5% SBS, no signifcant changes in stiffness are observed concerning a simple SBS modification. On the other hand, with 5% of μFA, the stiffness increases considerably with a greater impact at low temperatures, due to the hardening of the free binder and the contribution of the solid particles.

Figure 5 shows the |G*| master curves that demonstrate the increase in stiffness caused by the modifiers in the conventional binder. At high reduced frequencies (low temperatures) a leftward shift is generated by the modified binders because of the time-temperature superposition. For low ω_r (high temperatures) all modified binders have a theoretical projection of the curve higher than the conventional binder. This behavior would generate a better performance against plastic deformations or rutting. However, the projection on the master curve |G*| determines that the binder with 5%SBS would have higher values than a sample with 5%SBS+3% μFA. This is contradictory to the experimental data (see Table 5), where the sample with 3% of μFA has higher |G*| values. This is due to the slope that originates in the master curve when fitting the data, which is influenced by the clustering or dispersion of the |G*| data.

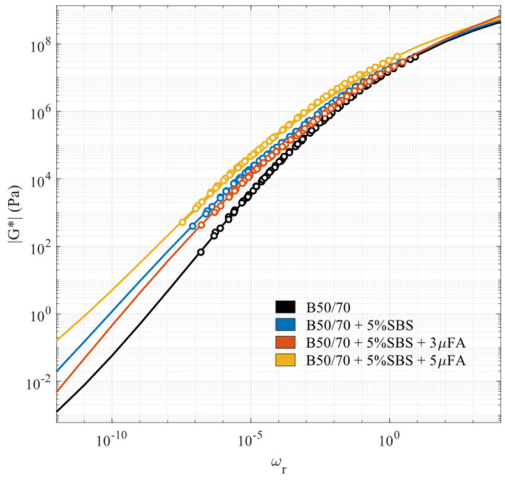

Figure 5. Master curves of the complex modulus |*G**|.

Preprints (www.preprints.org) | NOT PEER-REVIEWED | Posted: 21 December 2023 doi:10.20944/preprints202312.1644.v1

Table 5. Linear viscoelasticity parameters.

Sample	Variables	10°C	20°C	30°C	40°C	50°C	60°C	70°C
B50/70	|G*| (kPa)	10470,60	1957,60	324,67	64,08	12,47	3,35	1,04
	|G*|/sin(d) (kPa)	14306,15	2301,72	353,28	66,96	12,71	3,38	1,05
	|G*|·sin(d) (kPa)	7663,38	1664,93	298,38	61,33	12,23	3,33	1,04
B50/70 5%SBS	|G*| (kPa)	12353,60	2803,60	532,72	117,50	34,05	11,00	4,26
	|G*|/sin(d) (kPa)	18813,21	3608,50	626,54	135,65	38,52	11,86	4,45
	|G*|·sin(d)(kPa)	8111,93	2178,24	452,94	101,77	30,10	10,20	4,09
B50/70 5%SBS 3%mFA	|G*| (kPa)	12990,70	2784,68	574,81	141,96	41,10	12,62	4,37
	|G*|/sin(d) (kPa)	19277,19	3517,00	671,38	162,63	45,84	13,47	4,55
	|G*|·sin(d) (kPa)	8754,30	2204,85	492,13	123,92	36,85	11,81	4,20
B50/70 5%SBS 5%mFA	|G*| (kPa)	20311,90	4750,43	899,47	179,22	46,56	14,66	5,38
	|G*|/sin(d) (kPa)	32723,15	6292,15	1064,33	204,93	52,92	16,02	5,65
	|G*|·sin(d) (kPa)	12607,99	3586,47	760,15	156,74	40,97	13,42	5,12

Concerning the angle phase, it is observed that SBS generates a drastic change in the stress-strain relationship concerning the conventional binder (see Figure 6). B50/70 acquires the maximum consistency of δ=90° at 70°C, while the incorporation of 5%SBS manages to reduce δ to 65-76° for the same temperature. This shows that SBS modifies the internal structure of B50/70, generating greater elasticity in the LVE range. However, when adding μFA to the SBS-modified binder, no noticeable changes are generated (see Figure 6), showing that μFA only tends to increase the magnitude of the vector |G*| (see Table 5), keeping its elastic-viscous components practically constant. This condition would hypothetically demonstrate that the μFA with the B50/70+SBS binder interacts largely in a physical (agglomerating) and not chemical way.

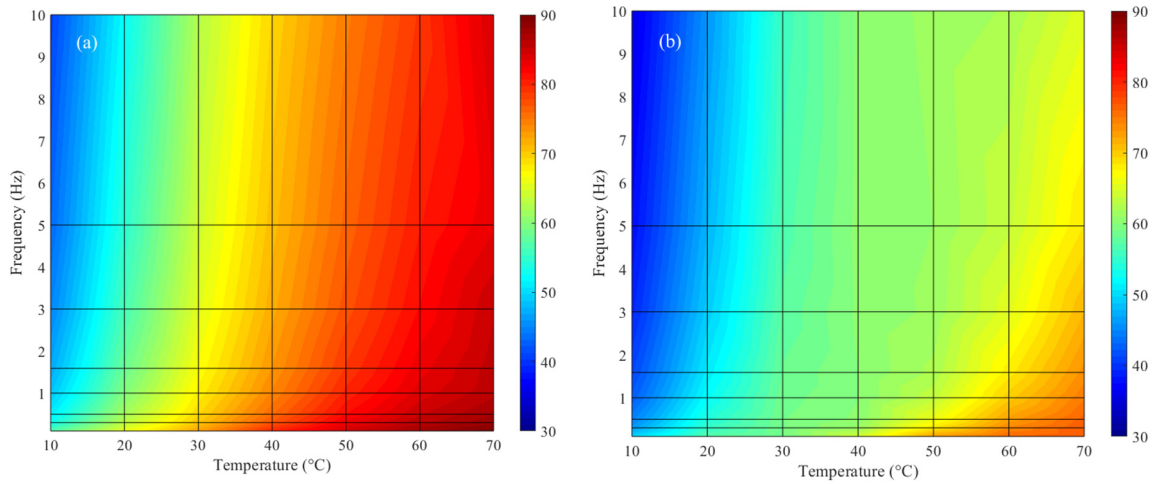

Preprints (www.preprints.org) | NOT PEER-REVIEWED | Posted: 21 December 2023 doi:10.20944/preprints202312.1644.v1

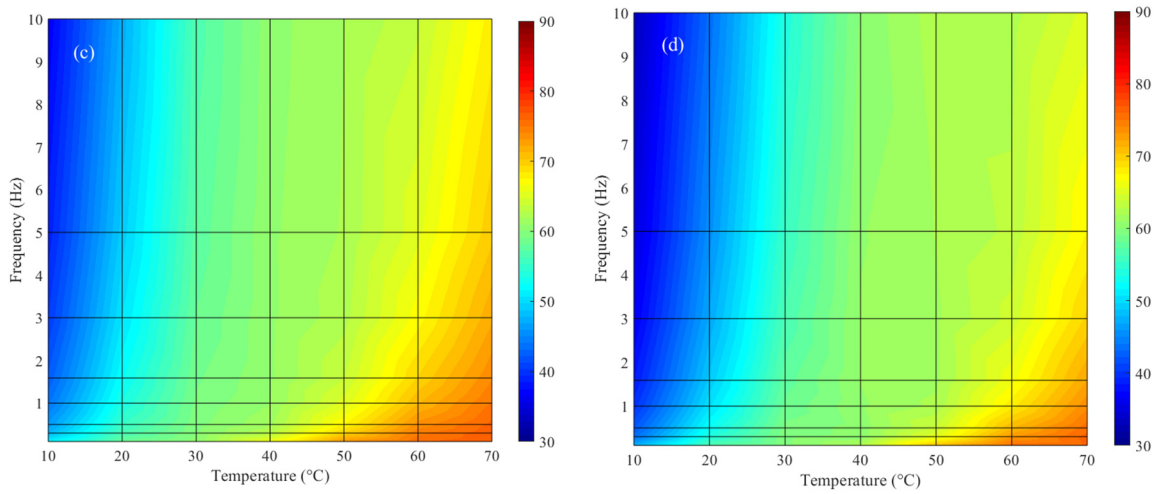

Figure 6. Angle phase d. a) B50/70; b) B50/70+5%SBS; c) B50/70+5%SBS+3mFA; d) B50/70+5%SBS+5mFA.

3.3. MSCR test

Figure 7 shows the results of the MSCR test. The increase in temperature generates a more significant deformation of the binders under study, which is directly proportional to the degree of penetration studied in section 3.1.

At 30°C, a behavior similar to that obtained in the LVE range is obtained (section 3.2), where the incorporation of SBS improves the performance considerably of binder B50/70. Adding 3% of µFA to the modified sample does not generate large changes in the accumulated deformation, where both samples have a plastic range Jnr of 20%. However, the addition of 5% µFA reduces the accumulated deformation concerning the other samples. This behavior is due to a greater amount of filler in the binder, which increases the stiffness of the sample and thus reduces the deformation. In addition, it is shown that the filler µFA has an impact on the creep phenomenon, modifying the maximum deformation reached. This behavior is relevant, since it is necessary to analyze the Jnr and R simultaneously because the variables alone do not demonstrate the general behavior of the sample. An example of this is the sample 5%SBS+5% µFA which has less accumulated deformation but presents a lower recovery R, compared to the sample 5%SBS+3% µFA (Table 6 and Figure 7a).

As the temperature increases, the deformation conditions are maintained. However, the sample with only SBS demonstrates higher deformations concerning those with µFA. For example, at 60°C the recovery loss conditions are high, where the sample with 5%SBS manages to exceed 1000% deformation, while the samples with 5%SBS+5% µFA and 5%SBS+3% µFA are below this value. For this specific case, the samples with µFA generate lower deformations in the creep phenomenon, and also a higher percentage recovery in each cycle as opposed to that demonstrated at lower temperatures (30°C).

Preprints (www.preprints.org) | NOT PEER-REVIEWED | Posted: 21 December 2023 doi:10.20944/preprints202312.1644.v1

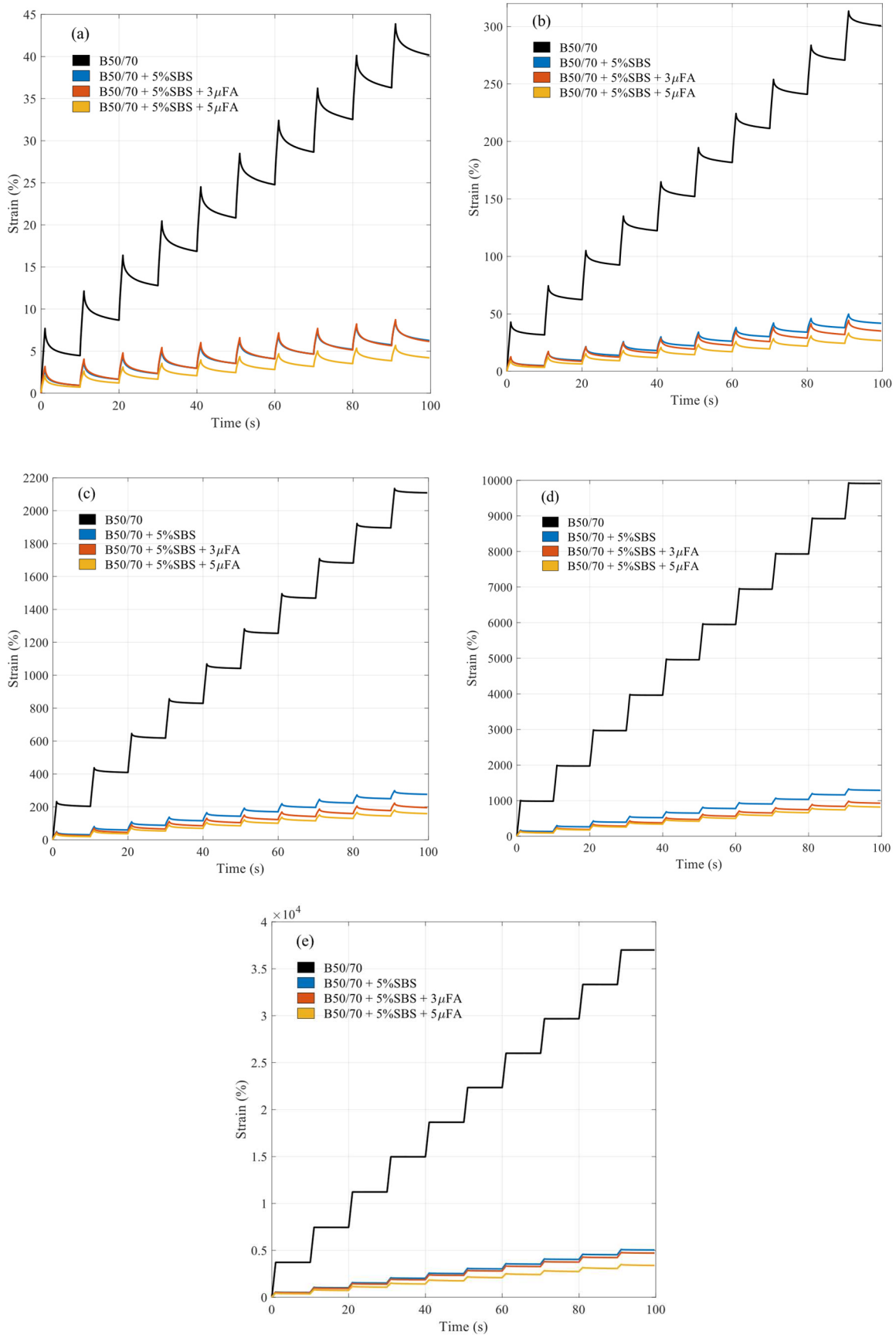

Figure 7. MSCR test. a) 30°C; b) 40°C; c) 50°C; d) 60°C; e) 70°C.

 doi:10.20944/preprints202312.1644.v1

Table 6. MSCR test parameters.

Temperature	Variables	B50/70	B50/70 5%SBS	B50/70 5%SBS 3%mFA	B50/70 5%SBS 5%mFA
30°C	Strain (%)	40,16	6,27	6,15	4,21
	R (%)	17,80	40,36	43,54	39,57
	J_{nr} (1/kPa)	1,25	0,20	0,20	0,13
40°C	Strain (%)	300,64	41,83	35,07	26,75
	R (%)	9,75	29,04	34,77	33,27
	J_{nr} (1/kPa)	9,39	1,31	1,10	0,84
50°C	Strain (%)	2108,47	276,14	195,24	159,01
	R (%)	3,73	16,16	23,36	22,81
	J_{nr} (1/kPa)	65,89	8,63	6,10	4,97
60°C	Strain (%)	9912,17	1290,28	927,95	819,29
	R (%)	0,56	7,31	13,58	13,09
	J_{nr} (1/kPa)	309,76	40,32	29,00	25,60
70°C	Strain (%)	37004,30	5036,79	4711,44	3386,70
	R (%)	0,26	3,16	4,16	6,95
	J_{nr} (1/kPa)	1156,38	157,40	147,23	105,83

3.4. LAS test

The LAS test evaluates the cracking of the asphalt binder using the VECD model, allowing estimation of the fatigue life of the samples in terms of shear deformation and accumulation of damage intensity. Figure 8 shows the stress-strain curves of the samples under study; the modified binders increase the maximum stress when SBS is incorporated. For example, at 20°C, the sample with only 5% SBS achieves σ_{max} with an increase of 44% compared to the conventional binder. In addition, it is observed that the base binder has a narrower σ_{max} compared to the modified binders, which would show a greater dependence on the applied deformation, resisting less fatigue. However, when 3% and 5% of μFA are added to the binder with 5% SBS, the σmax is also increased by 19% and 28%, respectively. But σ_{max} causes broader peaks, which could be attributed to the increase in the percentage of large molecules (SBS and μFA). In this sense, some authors have mentioned that a binder with a higher σ_{max} would be more prone to fracture. However, in the case of μFA, it is important to note that despite the σ_{max} they achieve wider curves, contributing to a lower dependence on deformation.

When increasing the temperature to 25°C, the samples reduce their stiffness with respect to 20°C. The conventional binder and the modification with 5% SBS increase the deformation for σ_{max}, which shows a more ductile behavior. However, by adding filler to the binder with SBS, the deformation does not increase for σ_{max}, but rather decreases for the case of 5% μFA due to the stiffening of the matrix, which increases the maximum stress but leads to premature failure (Table 7).

Preprints (www.preprints.org) | NOT PEER-REVIEWED | Posted: 21 December 2023 doi:10.20944/preprints202312.1644.v1

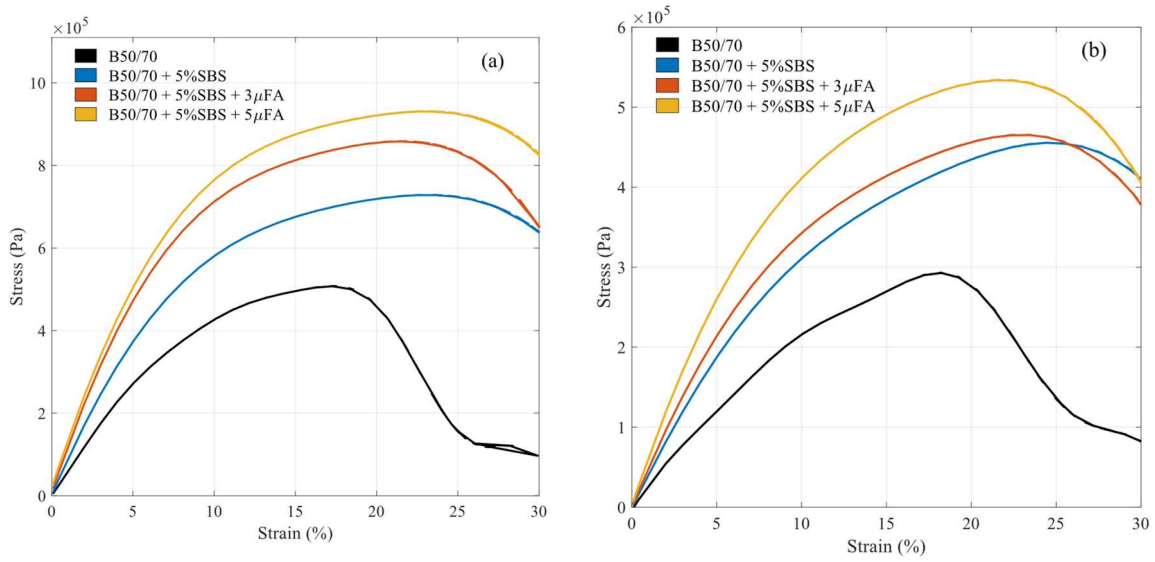

Figure 8. Stress-Strain Curves LAS: a) 20°C; b) 25°C.

When applying the VECD model, the energy dissipation resulting from the loss of structural integrity C caused by the accumulated damage intensity D. Figure 9 shows the integrity of the samples as the intensity D increases. At 20°C the base binder starts with a higher integrity than the modified binders, which is reduced as the intensity D increases. For example, the binder with 5%SBS acquires better C values over a D of 100 concerning B50/70, this behavior was also obtained δ in the LVE bond, where B50/70 achieves a premature softening. Even though B50/70 reduces its integrity notoriously, it is important to note that binders with 3% and 5% of µFA only acquire a better behavior compared to the conventional binder for a D higher than 176 and 255, respectively. This behavior is due to the higher stiffness of the binder modified with µFA, causing a higher maximum stress but with more brittleness.

As the temperature increases to 25°C, binders with 5%SBS and 5%SBS+3% µFA possess higher integrity from the start compared to B50/70. This could hypothetically be due to the ability of SBS to retard Newtonian fluid behavior. However, concerning the sample with 5% of µFA no better behavior is generated until a damage intensity of 123, which demonstrates the problem of viscoelastic material with too much stiffness at low temperatures. When comparing the complex modulus of the samples for the nonlinear viscoelasticity range, differences to what is observed in the LVE range are obtained. An example is the 5%SBS binder that achieves a |G*| of 3.8 MPa, versus the 4.4 MPa achieved by 5%SBS+3% µFA. This behavior is relevant since in the LVE range no significant difference was generated (see Table 5), so it can be inferred that the filler generates a greater impact when subjected to greater deformations. This may be due to a greater displacement of the binder matrix, generating that the solid particles of the microfiller (Figure 2b) achieve a greater influence.

Preprints (www.preprints.org) | NOT PEER-REVIEWED | Posted: 21 December 2023 doi:10.20944/preprints202312.1644.v1

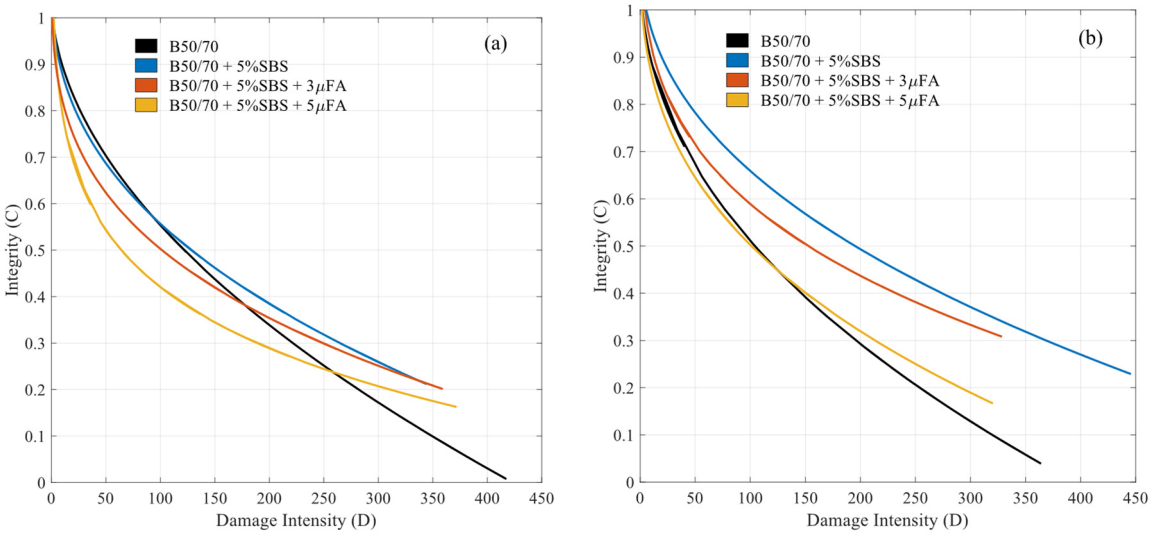

Figure 9. Material integrity vs. damage intensity: a) 20°C; b) 25°C.

The fatigue life *Nf* at 20°C and 25°C is shown in Figure 10. Binder B50/70 at any strain amplitude shows lower fatigue behavior. At 20°C the binders with 5%SBS and 5%SBS+3% μFA have similar behavior at low deformations, as the deformation amplitude increases the sample with only 5%SBS generates higher fatigue resistance. The binder with 5%SBS+5% μFA improves fatigue performance over the entire strain range. As the temperature increases by 5°C, the micro filler samples have worse fatigue performance than the SBS-only binder. This behavior is due to a higher stiffness of the samples with μFA, generating a higher brittleness. When comparing the samples with micro filler, it is observed that after a deformation amplitude of 5%, an abrupt decay is generated by the binder with 5%SBS+5% μFA. This behavior is attributed to the fact that the binder presents a drastic change in its stiffness, which caused an abrupt decay of the $|G^*| \cdot \sin(\delta)$ due to a possible premature failure.

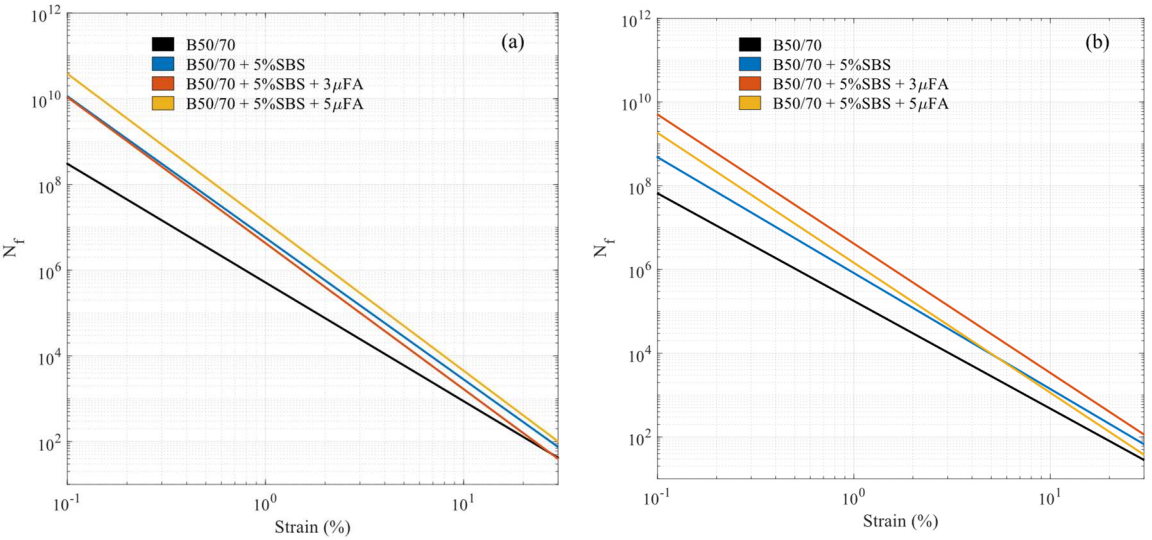

Figure 10. *Nf* for LAS test: a) 20°C; b) 25°C.

Preprints (www.preprints.org) | NOT PEER-REVIEWED | Posted: 21 December 2023 doi:10.20944/preprints202312.1644.v1

Table 7. LAS test parameters.

Temperature	Variables	B50/70	B50/70 5%SBS	B50/70 5%SBS 3%mFA	B50/70 5%SBS 5%mFA
20°C	a	1,38	1,65	1,7	1,73
	A	517000	5690000	4280000	13200000
	B	-2,77	-2,77	-3,41	-3,46
	k	1,53	1,78	2,03	2,02
	D_f	102	181	134	201
	$S_{máx}$	546473	818917	979366	1055270
	Strain	16,38	23,98	23,24	24,15
	$N_{2,5}$	40842	275459	188636	550618
	N_5	5988	27896	17778	49874
	$N_{7,5}$	1948	7308	4466	12240
	N_{10}	878	2825	1676	4518
25°C	a	1,29	1,38	1,54	1,55
	A	177000	823000	4150000	1450000
	B	-2,57	-2,77	-3,09	-3,11
	k	1,43	1,33	1,46	1,67
	D_f	72,1	147	202	129
	$S_{máx}$	308492	491099	503937	582975
	Strain	19,35	26,6	23,54	22,72
	$N_{2,5}$	16802	65006	244761	84204
	N_5	2824	9531	28779	9781
	$N_{5,5}$	995	3100	8227	2776
	N_{10}	475	1397	3384	1136

3.5. BYET test

Figure 11 shows the stress-strain curves of the BYET test for B50/70 and its modifications. The results show the same trends presented in the LAS test, where the addition of SBS and µFA increases the maximum stress reached (see Fig. 8). At 20°C, the maximum stress σ_{max} increases with the addition of 5% SBS by 275% concerning the base binder. On the other hand, when 3% µFA and 5% µFA are added, this stress increases by 62.67% and 84% concerning the binder with SBS, respectively. About the deformation reached by the samples in said σmax, it is observed that the deformation was reduced when adding a greater amount of micro filler in the sample. This is due to a higher brittleness of the samples with filler because of a higher stiffness in the binder matrix. This implies that the binder modified with µFA will resist fewer load repetitions and could fail earlier due to cracking at low temperatures. When analyzing Figure 11a, it is observed that when adding µFA and SBS, multiple peaks are obtained in the test, this behavior is pointed out by some authors as a reaction to the high elasticity and good recovery. Moreover, it has been defined that the first peak in the BYET test would indicate the asphaltene-maltene ratio, while the second peak would indicate the elastic capacity of the polymer.

As the temperature increases to 25°C (Figure 11b), the σ_{max} is reduced due to the softening of the binders. We observe that the multiple peaks occurring at 20°C are not generated, but the samples with µFA show a growth in stress after reaching the first peak. In this regard, it is hypothesized that the increase in temperature generates a greater displacement of the binder in the torque caused by

Preprints (www.preprints.org) | NOT PEER-REVIEWED | Posted: 21 December 2023 doi:10.20944/preprints202312.1644.v1

the DSR. In this way, the solid particles provide extra stiffness which could be defined as a reserve of the material. Thus, the increase in stiffness post-first peak would be due to the capacity of the micro filler μFA.

For this study, the creep energy (area under the curve) up to the point of the first peak in the graph was calculated. Table 8 indicates that the incorporation of SBS and μFA in the sample improved the *Er* of the base binder. The sample with 5%SBS+5% μFA is the one with the highest creep energy and thus would be able to resist plastic deformation and stresses before failure. However, it is important to note that this energy is calculated based on the Stress-Strain variables. With this, it should be emphasized that the deformation reached maximum stress is a direct indicator of the ductility and the capacity to resist loads. Which, for this study is inversely proportional to the creep energy.

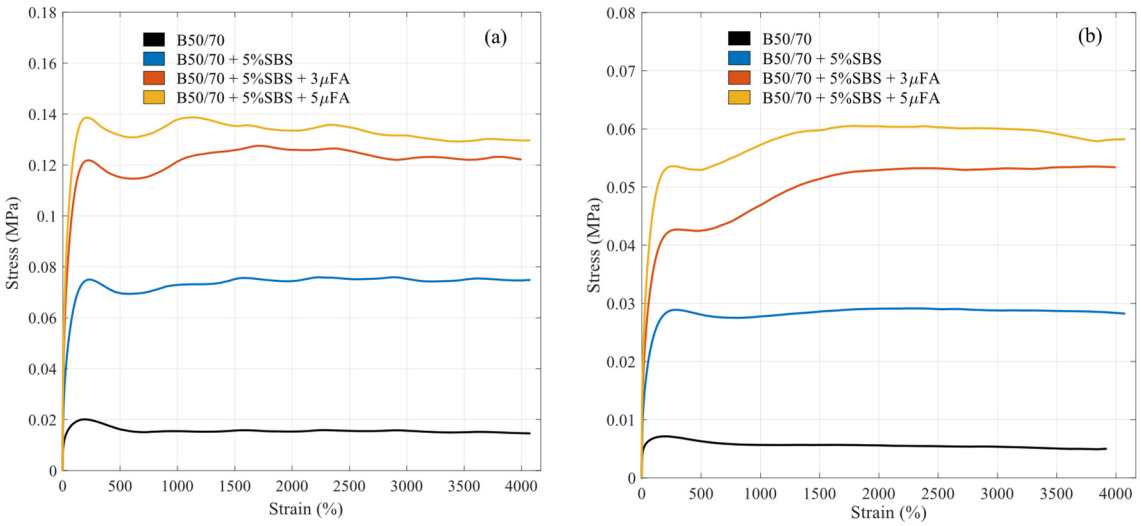

Figure 11. BYET test: a) 20ºC; b) 25ºC.

Table 8. BYET test parameters.

Temperature	Variables	B50/70	B50/70 5%SBS	B50/70 5%SBS 3%mFA	B50/70 5%SBS 5%mFA
20°C	s_{max} (MPa)	0,020	0,075	0,128	0,138
	Strain (%)	190,2	234,9	225,0	215,3
	E_r (MPa)	3.311	14,523	22,788	25,064
30ºC	s_{max} (MPa)	0,007	0,0288	0,042	0,054
	Strain (%)	192,7	298,3	288,5	249,64
	E_r (MPa)	1,244	7,329	10,417	11,215

3.6. Binder Draindown

Table 9 shows the results of the binder drainage of the PA asphalt mixes, in addition to the air void content and bulk density.

The results show that all tested samples meet the minimum binder drainage requirement (0.3% limit). This is relevant due to the low fine aggregate content of the PA mixes. It is found that adding μFA to the binder with 5% SBS results in a higher bulk density in the samples. However, the void content of the PA mixes is reduced (greater than 20%), due to a lower loss of the binder in the manufacturing process (Binder Draindown). This behavior is due to a higher binder consistency with

Preprints (www.preprints.org) | NOT PEER-REVIEWED | Posted: 21 December 2023 doi:10.20944/preprints202312.1644.v1

μFA, which has already been demonstrated by penetration, linear viscoelasticity, and progressive damage.

Table 9. Results for bulk density, air voids and binder runoff.

	Air Voids (%)	±Deviation (%)	Bulk density (gr/cm³)	±Deviation (gr/cm³)	Draindown test (%)
B50/70 + 5%SBS	23,13	1,12	1,992	0,028	0,20
B50/70 + 5%SBS + 3%mFA	22,66	1,01	2,004	0,025	0,07
B50/70 + 5%SBS + 5%mFA	22,45	1,28	2,009	0,032	0,04

3.7. Water sensitivity test

Figure 12a details the ITS results for dry and wet conditions, in addition to the ITSR index for PA mixes. None of the PA mixes meet the minimum requirement of an ITSR of 85%. However, when observing the results, it is observed that the incorporation of μFA increases this value, making the sample with 5% SBS the most vulnerable. When analyzing the samples independently, it is shown that the incorporation of μFA reduces the maximum stress reached in dry samples. This behavior is due to a higher stiffness of the sample that leads to an early indirect tensile rupture (Figure 12b). Concerning wet samples, there is no clear trend due to the incorporation of μFA.

For further details of the water sensitivity test on PA mixes. The Fracture Energy (FE) is calculated as the area under the curve up to σ_{max}, Post-Cracking Energy (PE) as the area under the curve after σmax, and finally, the toughness of the sample as the sum of FE and PE. For dry samples, it is obtained that FE is higher for the sample with 5%SBS with a value of 1307.9 (kPa·mm). Samples incorporating 3% μFA and 5% μFA reduce the FE energy of the 5%SBS binder by 33.22% and 31.43%, respectively. This reduction in energy causes the PA mixture with μFA to generate greater cracking before failure (σ_{max}). Regarding the PE energy, the sample with 5%SBS achieves a value of 1694.2 (kPa·mm). By adding filler μFA at 3% and 5%, the energy is reduced by 37.53% and 43.03%, respectively. This indicates that the higher the μFA content, the faster the crack propagation.

Concerning the wet samples, the PA with 5%SBS reduced its FE and PE energy compared to the dry condition. On the contrary, samples with 3% and 5% μFA increase the FE and PE energy in wet conditions. This increase is because the samples present higher ductility in the wet condition since the σ_{max} is achieved at higher deformations about the dry condition.

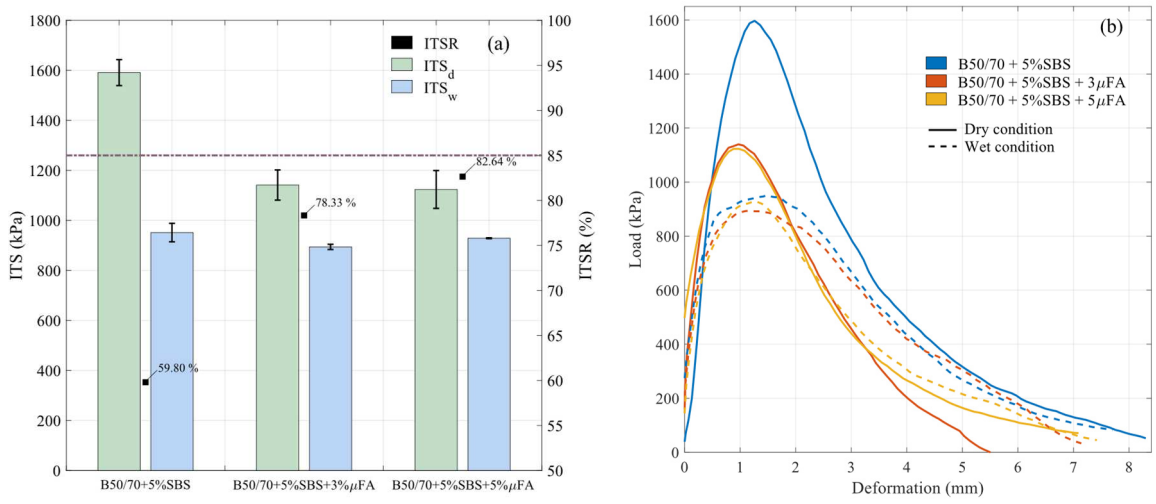

Figure 12. Results of Water sensitivity test: a) ITS and ITSR values; b) Load-deformation curve.

Preprints (www.preprints.org) | NOT PEER-REVIEWED | Posted: 21 December 2023 doi:10.20944/preprints202312.1644.v1

3.8. Cantabrian loss particle test (Dry and wet conditions).

The results of the Cantabrian test are shown in Figure 13 for dry and wet conditions. In dry conditions, the samples with 5%SBS+3% µFA and 5%SBS+5% µFA meet the requirement of having a particle loss of less than 20%. This result is relevant since one of the main concerns in the design of porous mixes is abrasion resistance. However, the sample with only 5% SBS generates a loss higher than this value of 21.4±3.5%. According to these results, the use of µFA in the binder matrix together with SBS can be used according to Spanish regulations for high traffic and hot areas for particle wear failure.

For wet conditions, all samples meet the requirement of a particle loss of less than 35%. In addition, it is observed that when incorporating a specific concentration of µFA the wear loss was higher, generating a maximum value of 26.2±8.3% for a sample with 5%SBS+5% µFA. On the other hand, it is again verified that the incorporation of µFA to the binder matrix generates a lower void content, but in no case less than 20%.

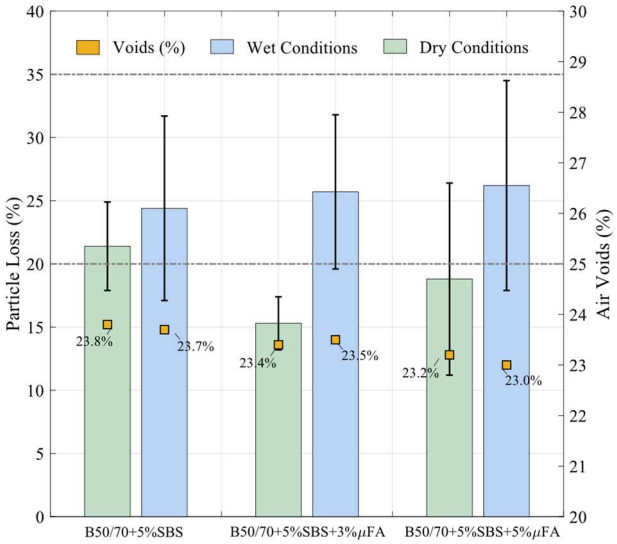

Figure 13. Results of Cantabrian loss particle test.

4. Conclusions

The research focuses on an experimental study of porous asphalt mixes with SBS-modified binder and fly ash micro filler. The study aims to determine the influence of fly ash micro filler (mFA) in Styrene-Butadiene-Styrene (SBS) modified binders for implementation in a PA16 mix. For this purpose, a rheological characterisation is carried out by analysing a conventional binder type B50/70 and comparing it with modified binders through penetration tests, DSR-test, MSCR, LAS and BYET. Subsequently, porous asphalt mixes are manufactured with the modified binders, considering a standard sample with 5% SBS, and tested for binder run-off and particle loss due to wear and water sensitivity. Based on the experimental results, the following conclusions are drawn:

- Based on the results obtained, it is validated that SBS improves the mechanical properties of the conventional binder, increasing the stiffness (G*|) and elasticity. In addition, it was found that by increasing the temperature, the increase in *d* is reduced, preventing premature softening of the binder. Based on the progressive damage tests, it is determined that SBS reduces the plastic range at high temperatures, increasing the R and decreasing the Jnr. Concerning low temperatures, SBS achieves remarkable behaviour by increasing the damage intensity *D*, generating a higher C integrity than the conventional binder. Also, SBS increases the fatigue life *Nf* and creep yield energy Er compared to the conventional binder.
- From rheological tests, adding mFA microfiller significantly improves the stiffness |G*| of SBS binders in the LVE range. However, the incorporation of mFA does not generate a noticeable

impact on d, which shows that its incorporation generates mainly a physical and not a chemical contribution. Concerning the MSCR test, mFA reduces all test temperatures for creep and recovery phenomena, performing better against permanent deformation and cupping. Based on the VECD simulation, mFA does not significantly affect the sample`s integrity with increasing damage intensity. In this sense, binders with mFA only achieve better C integrity for high damage intensities (D=176) than the base binder. Concerning the BYET test, the samples with mFA caused an increase in stress after reaching the first maximum stress at 25°C. The authors hypothesise that this behaviour is due to a higher displacement of the binder in the torque caused by the DSR. Thereby, the mFA particles provide extra stiffness, which could be defined as a reserve of the material.

- Based on the results of the PA16 porous mixes, adding mFA to the SBS-modified binder slightly reduces the percentage of voids in the sample (22.45%). This behaviour is because the samples with mFA produce a binder with a thicker film, generating a higher bulk density and less binder run-off. About abrasion resistance, it is concluded that all the samples meet the requirements in dry and wet conditions. However, the samples incorporating mFA in wet conditions achieve a higher particle loss with increasing concentration. In contrast, none of the PA samples meet the water sensitivity requirement. However, the addition of mFA manages to decrease the difference between dry and wet ITS. In the dry state, the samples with micro filler reduce the FE and PE energy due to higher cracking before failure and faster propagation after failure. In the wet state, the mFA samples increase the FE and PE energy due to higher ductility.
- Using FA micro filler as a secondary modifier in a polymeric binder with SBS improves the mechanical performance at the rheological level and other micro or nanomaterials studied in the literature review, such as clay or silica fume. On the other hand, it is concluded that the operating conditions in the binder modification process can affect the rheological properties and, thus, the future strength of the pavement. Therefore, implementing the fly ash microfiller as a second modifier at different dosages should be further investigated in future research for its correct technical and mechanical implementation and eventual economic improvement.

Author Contributions: Conceptualization, M.L-V. and D.M-Q.; methodology, M.L-V and D.M-Q.; software, M.L-V and M.V.; validation, M.L-V., D.M-Q. and AC.R.; formal analysis, M.L-V., D.M-Q. and AC.R.; investigation, M.L-V, M.V. and A.B.R-G.; resources, D.M-Q.; data curation, M.L-V.; writing—original draft preparation, M.L-V. and M.V. and A.B.R-G.; writing—review and editing, M.L-V and D.M-Q.; supervision, M.L-V., D.M-Q., AC.R. and D. C-F.; project administration, D.M-Q. All authors have read and agreed to the published version of the manuscript.

Funding: This research received no external funding.

Institutional Review Board Statement: Not applicable.

Informed Consent Statement: Not applicable.

Data Availability Statement: Data sharing is not applicable to this article.

Acknowledgements: The authors are grateful for the institutional support provided by the Faculty of Engineering Sciences of the Universidad Austral de Chile and the collaboration of the Polytechnic School of Zamora of the University of Salamanca.

Conflicts of Interest: The authors declare no conflict of interest.

References

1. E.J. Elizondo-Martínez, V.C. Andrés-Valeri, D. Jato-Espino, J. Rodriguez-Hernandez, Review of porous concrete as multifunctional and sustainable pavement, Journal of Building Engineering. 27 (2020). https://doi.org/10.1016/j.jobe.2019.100967.
2. A.M. Youssef, E.A. Fahmy, Evaluation of porous asphalt mixes stabilized by human scalp hair, Case Studies in Construction Materials. 19 (2023). https://doi.org/10.1016/j.cscm.2023.e02524.
3. J. Cai, C. Song, X. Gong, J. Zhang, J. Pei, Z. Chen, Gradation of limestone-aggregate-based porous asphalt concrete under dynamic crushing test: composition, fragmentation and stability, Constr Build Mater. 323 (2022). https://doi.org/10.1016/j.conbuildmat.2022.126532.

4. V.C. Andrés-Valeri, J. Rodriguez-Torres, M.A. Calzada-Perez, J. Rodriguez-Hernandez, Exploratory study of porous asphalt mixtures with additions of reclaimed tetra pak material, Constr Build Mater. 160 (2018) 233–239. https://doi.org/10.1016/j.conbuildmat.2017.11.067.
5. A.E. Alvarez, A.E. Martin, C. Estakhri, A review of mix design and evaluation research for permeable friction course mixtures, Constr Build Mater. 25 (2011) 1159–1166. https://doi.org/10.1016/j.conbuildmat.2010.09.038.
6. M. Lagos-Varas, D. Movilla-Quesada, A.C. Raposeiras, P. Monsalve-Cárcamo, D. Castro-Fresno, Rheological analyses of binders modified with triple combinations of Crumb-Rubber, Sasobit and Styrene-Butadiene-Styrene, Case Studies in Construction Materials. 19 (2023). https://doi.org/10.1016/j.cscm.2023.e02235.
7. F. Özel, M.T. Deniz, M.İ. Yüce, Evaluation of olive pomace and SBS modified bitumen to the performance characteristics, Case Studies in Construction Materials. 19 (2023). https://doi.org/10.1016/j.cscm.2023.e02432.
8. O.V. Laukkanen, H. Soenen, H.H. Winter, J. Seppälä, Low-temperature rheological and morphological characterization of SBS modified bitumen, Constr Build Mater. 179 (2018) 348–359. https://doi.org/10.1016/j.conbuildmat.2018.05.160.
9. B. Shirini, R. Imaninasab, Performance evaluation of rubberized and SBS modified porous asphalt mixtures, Constr Build Mater. 107 (2016) 165–171. https://doi.org/10.1016/j.conbuildmat.2016.01.006.
10. J. Liu, H. Li, J. Harvey, G. Airey, S. Lin, S.L.J. Lee, Y. Zhou, B. Yang, Study on leaching characteristics and biotoxicity of porous asphalt with biochar fillers, Transp Res D Transp Environ. 122 (2023). https://doi.org/10.1016/j.trd.2023.103855.
11. M. Lagos-Varas, D. Movilla-Quesada , A.C. Raposeiras, J.P. Arenas , M.A. Calzada-Pérez, P.L.-G. A. Vega-Zamanillo, Influence of limestone filler on the rheological properties of bituminous mastics through susceptibility master curves, Constr Build Mater. 231 (2020). https://doi.org/https://doi.org/10.1016/j.conbuildmat.2019.117126.
12. M. Lagos-Varas, D. Movilla-Quesada, A.C. Raposeiras, D. Castro-Fresno, O. Muñoz-Cáceres, V.C. Andrés-Valeri, M.A. Rodríguez-Esteban, Viscoelasticity modelling of asphalt mastics under permanent deformation through the use of fractional calculus, Constr Build Mater. 329 (2022) 127102. https://doi.org/https://doi.org/10.1016/j.conbuildmat.2022.127102.
13. Y. Tian, L. Sun, H. Li, H. Zhang, J. Harvey, B. Yang, Y. Zhu, B. Yu, K. Fu, Laboratory investigation on effects of solid waste filler on mechanical properties of porous asphalt mixture, Constr Build Mater. 279 (2021). https://doi.org/10.1016/j.conbuildmat.2021.122436.
14. B. Yang, H. Li, H. Zhang, L. Sun, J. Harvey, Y. Tian, Y. Zhu, X. Zhang, D. Han, L. Liu, Environmental impact of solid waste filler in porous asphalt mixture, Constr Build Mater. 303 (2021). https://doi.org/10.1016/j.conbuildmat.2021.124447.
15. D. Paul, M. Suresh, M. Pal, Utilization of fly ash and glass powder as fillers in steel slag asphalt mixtures, Case Studies in Construction Materials. 15 (2021). https://doi.org/10.1016/j.cscm.2021.e00672.
16. R.S. Blissett, N.A. Rowson, A review of the multi-component utilisation of coal fly ash, Fuel. 97 (2012) 1–23. https://doi.org/https://doi.org/10.1016/j.fuel.2012.03.024.
17. A.-R.S. SUHEIBANI, THE USE OF FLY ASH AS AN ASPHALT EXTENDER IN ASPHALT CONCRETE MIXES, 1986. https://www.proquest.com/dissertations-theses/use-fly-ash-as-asphalt-extender-concrete-mixes/docview/303423260/se-2?accountid=26778.
18. F. Li, Y. Yang, L. Wang, Evaluation of physicochemical interaction between asphalt binder and mineral filler through interfacial adsorbed film thickness, Constr Build Mater. 252 (2020) 119135. https://doi.org/https://doi.org/10.1016/j.conbuildmat.2020.119135.
19. R. Mistry, T.K. Roy, Effect of using fly ash as alternative filler in hot mix asphalt, Perspect Sci (Neth). 8 (2016) 307–309. https://doi.org/https://doi.org/10.1016/j.pisc.2016.04.061.
20. H. Fadil, D. Jelagin, M.N. Partl, A new viscoelastic micromechanical model for bitumen-filler mastic, Constr Build Mater. 253 (2020). https://doi.org/10.1016/j.conbuildmat.2020.119062.
21. M. El-Shafie, I.M. Ibrahim, A.M.M. Abd El Rahman, The addition effects of macro and nano clay on the performance of asphalt binder, Egyptian Journal of Petroleum. 21 (2012) 149–154. https://doi.org/10.1016/j.ejpe.2012.11.008.
22. C. Roman, M. García-Morales, Comparative assessment of the effect of micro- and nano- fillers on the microstructure and linear viscoelasticity of polyethylene-bitumen mastics, Constr Build Mater. 169 (2018) 83–92. https://doi.org/10.1016/j.conbuildmat.2018.02.188.
23. L.G.A.T. Farias, J.L. Leitinho, B. de C. Amoni, J.B.S. Bastos, J.B. Soares, S. de A. Soares, H.B. de Sant'Ana, Effects of nanoclay and nanocomposites on bitumen rheological properties, Constr Build Mater. 125 (2016) 873–883. https://doi.org/10.1016/j.conbuildmat.2016.08.127.
24. X. Shi, L. Cai, W. Xu, J. Fan, X. Wang, Effects of nano-silica and rock asphalt on rheological properties of modified bitumen, Constr Build Mater. 161 (2018) 705–714. https://doi.org/10.1016/j.conbuildmat.2017.11.162.

25. M. Fathi, A. Yousefipour, E. Hematpoury Farokhy, Mechanical and physical properties of expanded polystyrene structural concretes containing Micro-silica and Nano-silica, Constr Build Mater. 136 (2017) 590–597. https://doi.org/10.1016/j.conbuildmat.2017.01.040.
26. M. Lagos-Varas, A.C. Raposeiras, D. Movilla-Quesada, J.P. Arenas, D. Castro-Fresno, O. Muñoz-Cáceres, V.C. Andres-Valeri, Study of the permanent deformation of binders and asphalt mixtures using rheological models of fractional viscoelasticity, Constr Build Mater. 260 (2020). https://doi.org/10.1016/j.conbuildmat.2020.120438.
27. M. Lagos-Varas, D. Movilla-Quesada, A.C. Raposeiras, D. Castro-Fresno, Á. Vega-Zamanillo, M. Cumian-Benavides, Use of Hydrated Ladle Furnace Slag as a filler substitute in asphalt mastics: Rheological analysis of filler/bitumen interaction, Constr Build Mater. 332 (2022) 127370. https://doi.org/https://doi.org/10.1016/j.conbuildmat.2022.127370.
28. P. Lastra-González, I. Indacoechea-Vega, M.A. Calzada-Pérez, D. Castro-Fresno, A. Vega-Zamanillo, Mechanical assessment of the induction heating as a method to accelerate the drying process of cold porous asphalt mixtures, Constr Build Mater. 208 (2019) 646–650. https://doi.org/10.1016/j.conbuildmat.2019.03.053.
29. C.J. Slebi-Acevedo, P. Lastra-González, I. Indacoechea-Vega, D. Castro-Fresno, Laboratory assessment of porous asphalt mixtures reinforced with synthetic fibers, Constr Build Mater. 234 (2020). https://doi.org/10.1016/j.conbuildmat.2019.117224.
30. V.S. Arrieta, J.E.C. Maquilón, Resistance to Degradation or Cohesion Loss in Cantabro Test on Specimens of Porous Asphalt Friction Courses, Procedia Soc Behav Sci. 162 (2014) 290–299. https://doi.org/10.1016/j.sbspro.2014.12.210.